academicJournals

Vol. 9(11), pp. 211-222, November, 2015
DOI: 10.5897/AJPAC2015.0656
Article Number: EE1CD6956202
ISSN 1996 - 0840

http://www.academicjournals.org/AJPAC

African Journal of Pure and Applied Chemistry

Full Length Research Paper

Synthesis, characterization and photocatalytic activity of $MnO_2/Al_2O_3/Fe_2O_3$ nanocomposite for degradation of malachite green

Haile Hasana Logita[1]*, Abi Tadesse[2] and Tesfahun Kebede[2]

[1]Chemistry Department of Hawasa College of teacher education, Ethiopia.
[2]Chemistry Department of Haramaya University, Ethiopia.

Received 1 October, 2015; Accepted 22 October, 2015

New nanocomposite $MnO_2/Al_2O_3/Fe_2O_3$ photocatalyst was successfully synthesized by sol-gel method using metal salts as precursors in the presence of acid catalyst. The as-synthesized samples were characterized by X-ray diffraction (XRD), Fourier transform infrared (FTIR), atomic absorption spectroscopy (AAS) and UV-Vis diffuse reflectance spectroscopy. Elemental analyses of the as-synthesized samples were similar to those expected from the initial concentrations of the solutions used during synthesis. The x-ray diffraction pattern indicated that all as-synthesized samples had a crystal size with a rhombohedral structure and finest particle size of the catalyst (20.096 nm) was obtained at 400°C calcination temperature. The band gap energy of the $MnO_2/Al_2O_3/Fe_2O_3$ photocatalyst was calculated to be 1.97 eV and indicated that the as-synthesize sample had high photoabsorption property in the visible light region. Fourier transform infrared spectra confirmed the presence of hydroxyl group and Fe-O bond vibration in the catalyst. Experimental result of the $MnO_2/Al_2O_3/Fe_2O_3$ photocatalyst calcined at 400°C in 180 min (the molar ratio of 10 wt% Mn/15 wt% Al/75 wt% Fe) exhibited high photocatalytic activity of 92.89% under visible light irradiation. This may be due to the coupling effect of semiconductors, small particle size of catalyst and low electron-hole pair recombination on the surface of the catalyst. The pseudo-first-order rate constants of MG dye degradation in the presence of the catalyst were calculated as 4×10^{-4}, 6.56×10^{-3} and 1.0×10^{-2} min^{-1} under no light irradiation, UV and visible light irradiation, respectively.

Key words: Malachite green, nanoparticles, photocatalysis, sol-gel synthesis, ternaryoxides.

INTRODUCTION

Heterogeneous photocatalysis has become an alternative treatment method for degradation of organic pollutants from wastewater, which has the ability to mineralize organic compounds. In fact, photocatalysis can greatly contribute to the remediation of those environmental pollutants into environmental friendly species: CO_2, H_2O

*Corresponding author. E-mail: julianacr@epamig.ufla.br.

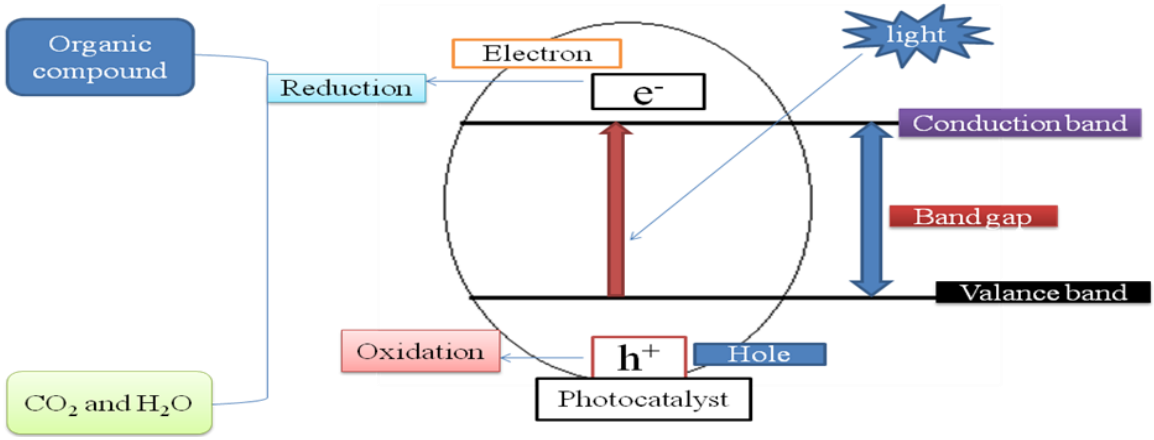

Figure 1. Schematic diagram of photocatalytic process initiated by photon acting on the semiconductor.

or other oxides, halide ion, phosphate (Sakthivel et al., 2005; Brijesh et al., 2008; Gomathi et al., 2009). The semiconducting metal oxides like iron oxide (Fe_2O_3) nanomaterials exhibit promising photocatalytic activities due to their environmental friendly behavior, low catalyst cost, high specific surface area, high crystallinity and solar energy application (Leland and Bard, 1987; Zhao et al., 2009; Bharathi et al., 2010) and thus, could be an alternative material for environmental application and wastewater treatment (Rhoton et al., 2002; Lei et al., 2006, 2007; Wang et al., 2009). However, the photocatalytic activity of the iron oxide is depending on the particle size, which is difficult to synthesize nano-sized iron oxide by conventional method and to control its crystal size in the photocatalyst (Park et al., 2010). This is due to the agglomeration of nano-particles in the aqueous solution, which causes the reduction of photocatalytic efficiency. This therefore warrants some smart strategy for use of iron oxide catalyst. One certain way to overcome this drawback is to apply innovative synthetic method of iron oxide nanoparticles of the catalysts that can be easily dispersed in organic medium and homogenously loaded on to the supported materials.

Many studies have continuously tried to improve the photocatalytic activity of iron oxide by coupling of different semiconductor oxide nanoparticles (Baldrian et al., 2006; Laat and Le, 2006; Kitis and Kaplan, 2007; Zelmanov and Semiat, 2008). Thus Al_2O_3/Fe_2O_3 supported photocatalyst has shown a better photocatalytic activity (El-Moselhy, 2009; Li et al., 2010; Pattanayak, 2010; Jia-feng et al., 2011). These new composite allows for the decreasing of the particle size of the catalyst (Karakassides and Gournis, 2003). It is an important material for the application of heterogeneous photocatalysis (Cordier et al., 2006). However, the photocatalytic activity of Al_2O_3/Fe_2O_3 nanocomposite is still not satisfactory for degradation of organic pollutants in wastewater because of its low electron-hole separation. This may be due to similar ionic radii and same charge of the materials. Subsequently complete substitutions occur between aluminum (III) oxide and iron (III) oxide nanoparticles and no structural defect could be expected (Neiva et al., 2009). Currently, nano-manganese (IV) oxide (MnO_2) has received a great potential application in environmental protection and degradation of organic pollutants in wastewater (Mitta et al., 2009; Su, 2010). It is a promising material for heterogeneous photocatalyst as a new generation environmental friendly catalyst. This is due to its high specific surface area, crystallinity, ability to disintegrate water molecule into hydrogen and hydroxide ions (Kang et al., 2007; Chu and Zhang, 2009). Based on these advantages MnO_2 semiconductor was chosen as an assistant component of photocatalyst to improve the photocatalytic activities of binary Al_2O_3/Fe_2O_3 nanocomposite. Therefore, in this study the triple oxide photocatalyst of $MnO_2/Al_2O_3/Fe_2O_3$ was used in photodegradation of MG dye in aqueous solution by using atomic absorption spectroscopy (AAS), X-ray diffraction (XRD), Fourier transform infrared (FTIR) and UV/Vis spectrometric techniques. A schematic representation of the photocatalytic process is represented in Figure 1.

MATERIALS AND METHODS

Synthesis of photocatalyst

The $MnO_2/Al_2O_3/Fe_2O_3$ ternary mixed nanoxide powder was prepared by sol-gel method. The sol corresponded to total volume ratio of metal, butanol, deionized water and nitric acid ratio of 1:20:4:0.1. In each case, ferric nitrate nanohydrate and aluminum nitrate nanohydrate were dissolved in stoichiometric amounts of water, 69% HNO_3 and butanol then mixed with vigorous stirring. $KMnO_4$ and $Na_2S_2O_3.5H_2O$ were mixed with each other and dissolved in double dionized water to form dark-brown MnO_2 solution. Subsequently, the dark brown MnO_2 solution was added drop wise into the mixture of aluminum oxide/iron oxide solution through stirring for 30 min at room temperature. The prepared sol was left to stand for the formation of gel. After the gelation was completed, the gel was aged for 5 days at room temperature and

Table 1. Designation of the as-synthesized powders.

Sample code	Precursor composition in g	%Composition at different calcination temperature
T_1	Al-3.64/Fe-36.46	90% Fe/10 % Al/0% Mn calcined at 400°C
T_2	Mn-0.83/Al-5.46/Fe-32.41	80% Fe/15 %Al/5% Mn calcined at 400°C
T_3	Mn-1.66/Al-5.64/Fe-30.38	75% Fe/15 % Al/10%Mn calcined at 400°C
T_4	Al-3.64/Fe-36.46	90% Fe/10 % Al/0% Mn calcined at 600°C
T_5	Mn-0.83/Al-5.46/Fe-32.41	80% Fe/15 %Al/5% Mn calcined at 600°C
T_6	Mn-1.66/Al-5.64/Fe-30.38	75% Fe/15 % Al/10% Mn calcined at 600°C

sample was dried at 75°C for 36 h. After grinding the dried samples, they were calcined at 400 and 600°C for 3 h at the different molar ratios. The different molar ratios of MnO_2:Al_2O_3:F_2O_3 are summarized in Table 1.

Characterization

Elemental composition

The elemental compositions of the as-synthesized powder were analyzed by flame atomic absorption spectrophotometer. 0.01 g of the as-synthesized powders were digested with conc. HNO_3 (7 ml), conc. HCl (4 ml) and H_2O_2 (2 ml) using acid digestion tube till clear solution appeard. The samples of Fe (III) and Mn (IV) solutions were transferred to 100 and 50 ml volumetric flasks and brought to volume using de-ionized water; triplicate solutions of iron and manganese were read from 100 and 50 ml volumetric flasks, respectively. Stock standard solutions of 1000 mg/L Fe and Mn were prepared by dissolving 0.14 and 0.36 g of corresponding salts in de-ionized water, respectively and series standard solutions were prepared to plot the calibration curves of the metals by appropriate dilution.

X-ray diffraction study

In order to determine the crystal phase composition of as-synthesized photocatalysts, all powder catalysts were ground to fine particles and analyzed by a BRUKER D8 Advance XRD, AXS GMBH, Karlsruhe, West Germany X-ray diffractometer (XRD) equipped with a Cu target for generating a Cu Kα radiation (λ = 0.15406 nm) at GSE. The accelerating voltage and the applied current were 40 kV, 30 mA, respectively. The instrument was operated under step scan mode with step time and degree (2θ) of 1 s and 0.020°, respectively for the range of 4 to 64°.

UV-Visible diffuse absorbance

For the estimation of absorption edge of the as-synthesized photocatalyst, UV-Visible diffuse absorption was measured using SP65 spectrophotometer at Addis Ababa University research laboratory. As-synthesized sample was dissolved in hot methanol then the UV-Visible diffuse absorbance of the powder was recorded at 200 to 800 nm range to determine the band gap of the photocatalyst.

Fourier transform infrared study

As-synthesized nanopowder was characterized using FTIR (SHIMIDAZU) instrument. Ten mg (dry mass) of the photocatalyst was thoroughly mixed with 100 mg (dry mass) of KBr and ground to a fine powder. A transparent disc was formed by applying a pressure in moisture-free atmosphere. The IR absorption spectrum was recorded between 400 and 4000 cm^{-1}.

Photocatalytic degradation studies

Photocatalytic activities of the as-synthesized powder were evaluated by decolorization of malachite green dye in aqueous solution. The experiments were carried out in the presence of UV and Visible light irradiation without any catalyst (blank), with catalyst in dark and in the presence of $MnO_2/Al_2O_3/Fe_2O_3$ photocatalyst. The photocatalytic reactor consists of a Pyrex glass beaker with an inlet tube for provision of air purging during photocatalysis and outlet tube for the collection of samples from the beaker as shown in Figure 2. Reaction was set up by adding 0.15 g of the as-synthesized powder into 100 ml of MG solution (25 mg/L) in the Pyrex glass beaker of 250 ml volume and the suspension was magnetically stirred in dark for 30 min to obtain adsorption/desorption equilibrium before irradiating the light in the beaker. Before illumination of the samples by UV or visible radiations, air/oxygen was purged into the solution with the help of a porous tube at hand purging in order to keep the suspension of the reaction homogenous. During the reaction, the solution was maintained at room temperature and the distance of the lamp from the solution was 9 cm and its intensity was recorded to be 8.25 MW/cm^2. Then, the light source was activated; 10 ml of the sample was withdrawn at 20 min time interval over irradiation time for 180 min. The suspension was centrifuged at 3000 rpm for 10 min and filtered to remove the catalyst particles before measuring absorbance. The absorbance of the clear solution was measured at a λ_{max} of 620 nm for quantitative analysis. The UV lamp with a definite power 12 W, 230 V and 50 Hz frequency was employed as UV light source, and incandescent bulb was used as visible light source with a definite power of 40 W, 220 V and 60 Hz frequency. Percentage degradation of MG dye was calculated using the following relation:

$$\%\,\text{Degradation} = \frac{A_o - A_t}{A_o} \text{x} 100$$

Where: A_0 is absorbance of dye at initial stage, A_t is absorbance of dye at time t.

RESULTS AND DISCUSSION

Characterization

Elemental composition

Elemental compositions of the as-synthesized samples

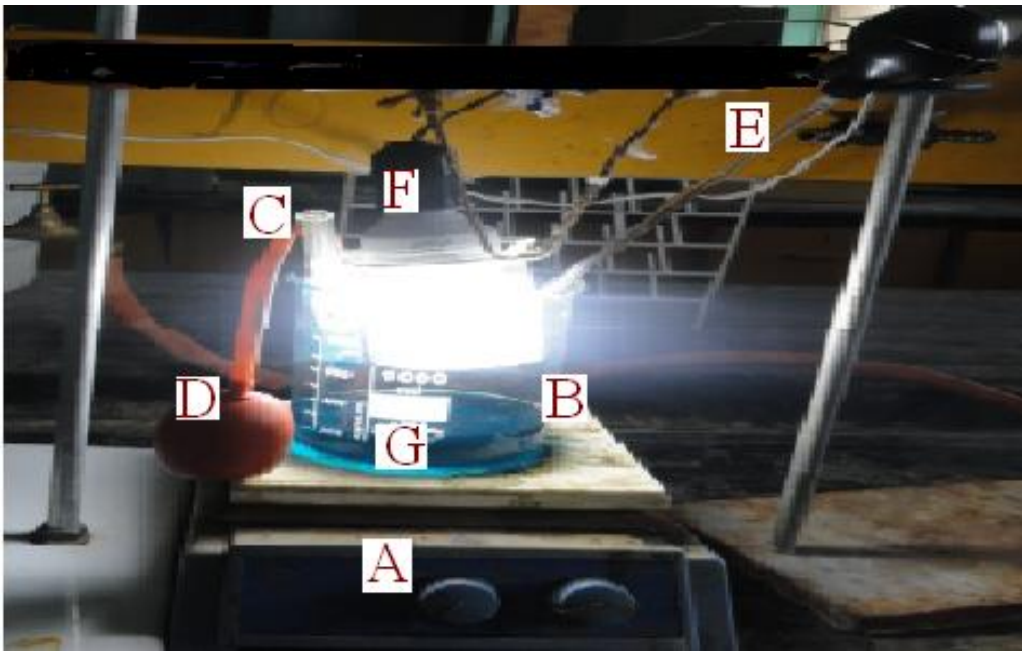

Figure 2. Schematic diagram of photocatalytic reaction in pyrex glass beaker under visible light irradiation. A. Hot plate (B) Pyrex glass beaker containing the solution (C) Inlet tube for air purging (D) Porous tube (E) Outlet tube for collecting sample solutions at 20 min time interval (F) Radiation source (G) Magnetic stirrer.

Table 2. Percentage composition of Iron oxide and Manganese oxide were calculated from as-synthesized powders

Sample name	%Fe[a]	%Fe[b]	%Mn[a]	%Mn[b]	%Al[a]	%Al[b]
Al_2O_3/Fe_2O_3	90	90.50	0.00	0.00	10	-
$MnO_2/Al_2O_3/Fe_2O_3$	80	81.58	5.00	4.66	15	-
$MnO_2/Al_2O_3/Fe_2O_3$	75	75.79	10	10.62	15	-

[a]initial percentage composition of as-synthesized sample, [b]percentage composition of as-synthesized sample calculated from the AAS and %Al[b] not determined.

were analyzed through flame atomic absorption spectrophotometer. Triplicate sample solutions were carried out together with blank solution on each sample as shown in Table 2. The standard solutions of iron and manganese metals were analyzed and the calibration curves were plotted on standard solution versus absorbance. Accordingly, the percentage composition of iron and manganese oxide analyzed by AAS was similarly to those expected from the initial concentration of the solution that was measured during the synthesis.

X-ray diffraction analysis

The crystallinity of the Al_2O_3/Fe_2O_3 and $MnO_2/Al_2O_3/Fe_2O_3$ photocatalysts synthesized by the sol-gel method at different molar ratios were studied by XRD after calcination at 400 and 600°C. The broad diffraction peaks presented in Figures 3 and 4 clearly revealed that all as-synthesized samples were nanosized crystals with a rhombohedral structure of hematite. Similarly, weak diffraction peaks presented in all as-synthesized samples at 2θ values of 24.1, 35.6, 40.8, 49.3, 54.0 and 62.3 were due to Fe_2O_3, and these correlated with the reported data of hematite (Park et al., 2010). However, the XRD data did not show any presence of Al_2O_3 and MnO_2 particles in the ternary mixed oxide system which confirmed that Al (III) and Mn (IV) enter into the Fe_2O_3 lattice substitution. In fact, ionic radius of Mn (IV) of 53 pm and Al (III) of 54 pm is similar to that of ionic radius (55 pm) of Fe (III) thus the substitution in the matrix of Fe_2O_3 is a favorable process. As a result, Al (III) ions and Mn (IV) ions can substitute Fe (III) lattice site to form a stable solid solution. The average crystallite sizes of the as-synthesized powders were calculated using Debye Scherer equation (Yan et al., 2010):

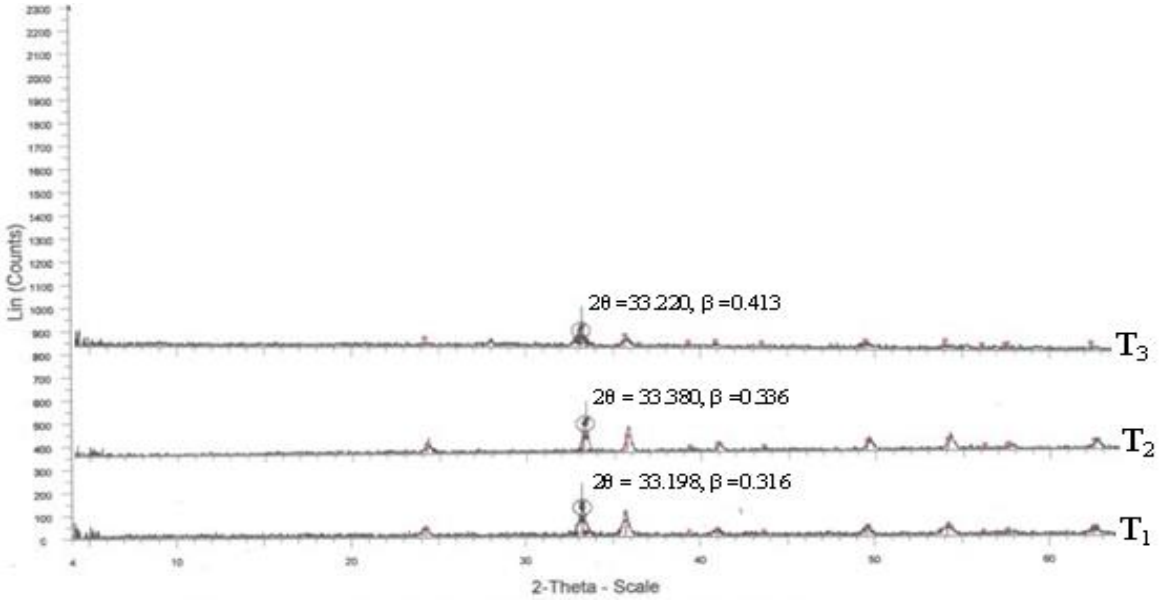

Figure 3. X-ray powder diffraction of the photocatalyst after calcination at 400°C

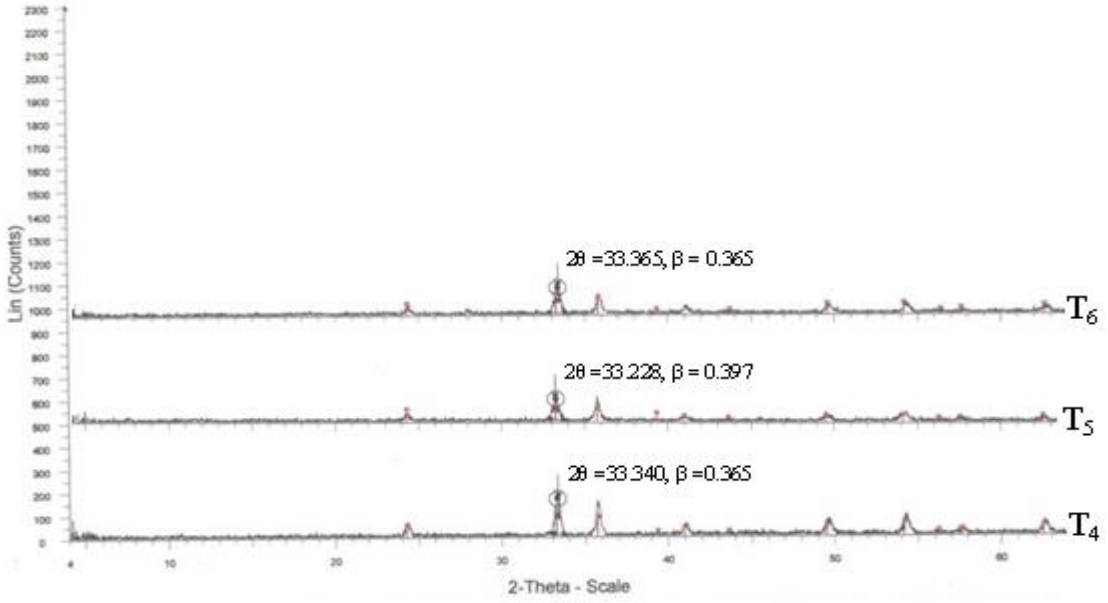

Figure 4. X-ray powder diffraction of the photocatalyst after calcination at 600°C.

$$D = \frac{K\lambda}{\beta cos\theta}$$

Where D is the crystal size (nm), λ is X-ray wavelength corresponding to the Cu target Kα irradiation (0.15406 nm), and β is full width at half maximum (FWHM) of the peak in radian, K = 0.90 is a constant coefficient of spherical shape and θ is the (Bragg angle) corresponding to the diffraction angle. The calculated average crystallite sizes (D) of the photocatalysts are given in Tables 3 and 4.

As shown from the tables, all the as-synthesized powders were nanosized crystal and sample T_3 of Mn-1.66/Al-5.64/Fe-30.38 calcined at 400°C has the smallest crystalline size and hence a high surface area. This sample was selected for UV-Visible and FTIR characterization and photodegradation experiment of malachite green.

Table 3. Average particle size (D) of the as-synthesized nanopowder calcined at 400°C.

Sample code	Precursor composition (g)	2θ(Degree)	β(Radian)	D(nm)
T_1	Al-3.64/Fe-36.46	33.198	0.316	26.310
T_2	Mn-0.83/Al-5.46/Fe-32.41	33.380	0.336	24.760
T_3	Mn-1.66/Al-5.64/Fe-30.38	33.220	0.413	20.096

Table 4. Average particle size (D) of the as-synthesized nanopowder calcined at 600 ^{0}C

Sample code	Precursor composition (g)	2θ(Degree)	β(Radian)	D(nm)
T_4	Al-3.64/Fe-36.46	33.340	0.365	24.531
T_5	Mn-0.83/Al-5.46/Fe-32.41	33.228	0.397	24.530
T_6	Mn-1.66/Al-5.64/Fe-30.38	33.365	0.365	22. 620

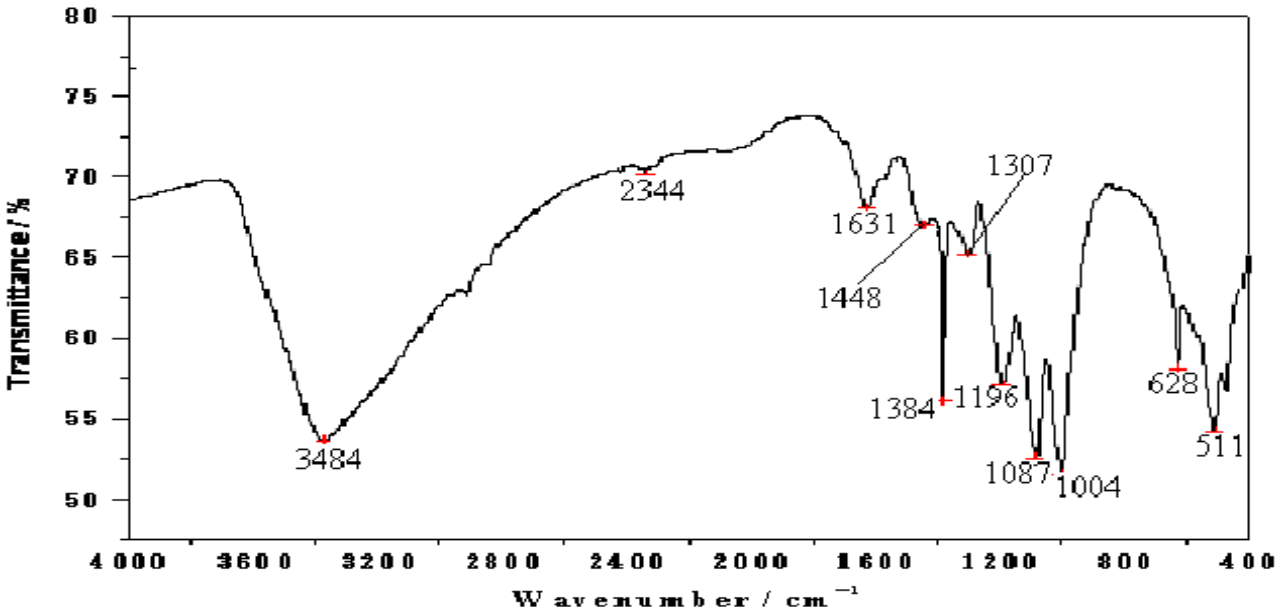

Figure 5. FTIR spectra of $MnO_2/Al_2O_3/Fe_2O_3$ nanopowder before calcinations.

FTIR analysis of photocatalysts

The FTIR spectra of the nanocomposite $MnO_2/Al_2O_3/Fe_2O_3$ photocatalyst prepared by sol-gel method before and after calcination are presented in Figures 5 and 6. The intense band at 3384 cm^{-1} may be due to the stretching modes of -OH group from adsorbed water in the sample. The band observed at 1631 cm^{-1} can be assigned to the bending vibration of free water molecule; while bands observed at 2344, 1448, 1384 and 1307 cm^{-1} may be attributed to -CH, $-CH_2$ and $-CH_3$ functional groups. Sharp peaks at 1196, 1087 and 1004 cm^{-1} may be due to C-O stretching vibration of primary alcohol, which was used to support the sol gel synthesis. The absorption peak observed at 628 cm^{-1} could be associated with the presence of Fe-O bond in the catalyst structure. The band at 511 cm^{-1} may indicate the presence of iron oxide in $MnO_2/Al_2O_3/Fe_2O_3$. Broad band at 3440 cm^{-1} may be due to the stretching vibration of -OH from adsorbed water in the crystal sample. The band observed at 1623 cm^{-1} could be assigned to the bending vibration mode of free water molecule. Weak bands observed at 2925, 2850 and 1384 cm^{-1} may be due to C-H stretching vibrations of primary alcohol. The peaks at 486 and 553 cm^{-1} may be attributable to the Fe-O vibration bond of hematite in the $MnO_2/Al_2O_3/Fe_2O_3$ nanocomposite of rhombohedral structure (Li et al., 2007).

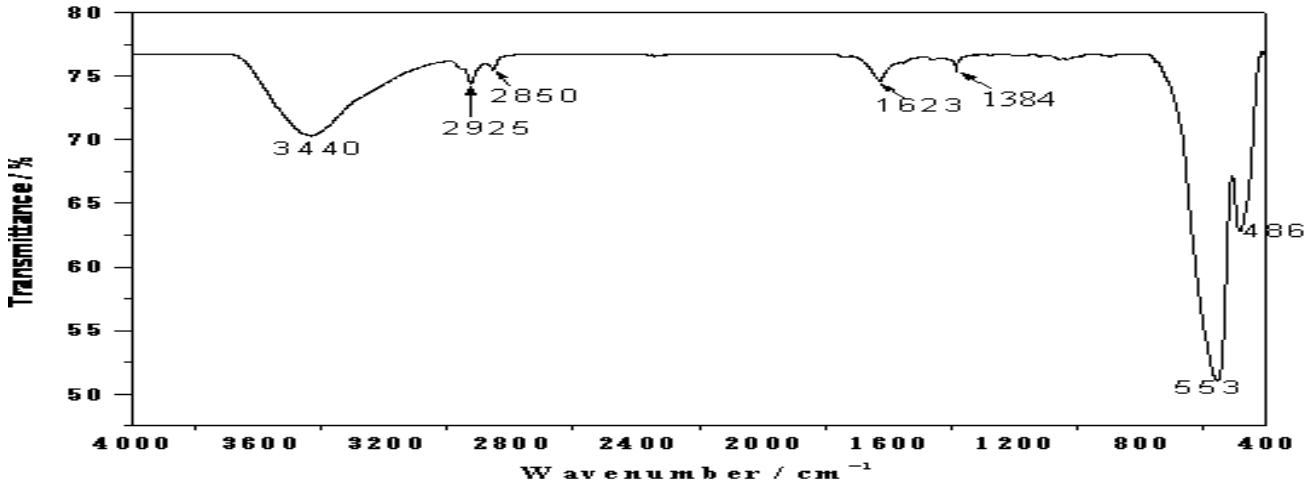

Figure 6. FTIR spectra of $MnO_2/Al_2O_3/Fe_2O_3$ nanopowder after calcination at 400°C.

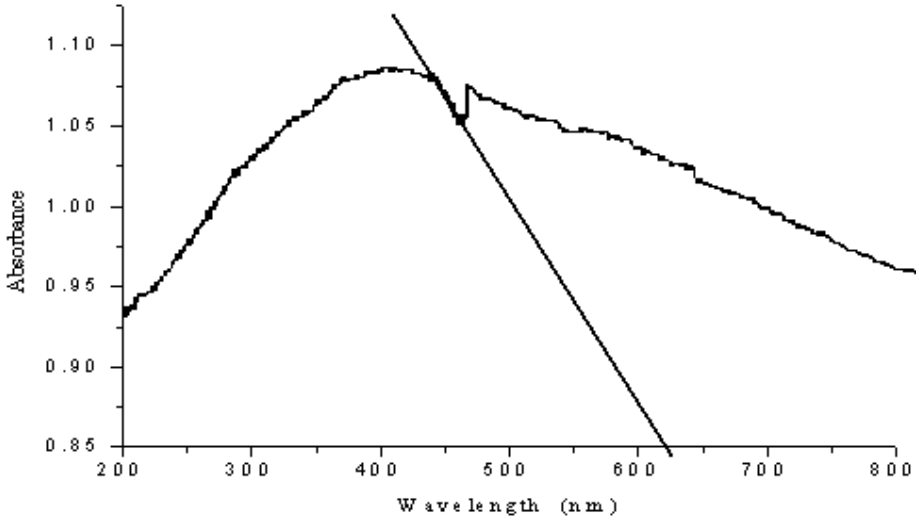

Figure 7. UV-Visible absorption spectra of as-synthesized photocatalyst $MnO_2/Al_2O_3/Fe_2O_3$.

Generally, from the FTIR spectra shown in the Figure 6, it can be concluded that intensities of most of the vibration peaks have eventually decreased during the conversion process of the precursors into the $MnO_2/Al_2O_3/Fe_2O_3$ photocatalyst. This change may be attributed to the decomposition of organic substances present before the calicination and the formation of crystalline phase during the process of heat treatment. As a consequence, only the vibration band corresponding to a Metal-Oxygen bond could be detected below 700 cm^{-1} (Torres-Martinez et al., 2010).

UV-Visible diffuse absorption edge

The optical absorption property of the material and migration of the light induced electrons and holes are considered as the key factor controlling the photocatalytic reaction. Of course, these migrations are relevant to the change in the electronic structure and characteristic of the material. The UV-Vis diffuse reflectance spectra of the as-synthesized $MnO_2/Al_2O_3/Fe_2O_3$ nanopowder obtained by the sol gel method and calcined at 400°C for 3 h was subjected to strong photoabsorption in the visible light region as shown in Figure 7. On the basis of this, the band gap energy (E_g) of the material can be calculated using the following formula (Chien-Tsung, 2007):

$$E_g(eV) = \frac{1240}{\lambda}$$

Where E_g is band gap energy in electron volt, λ is

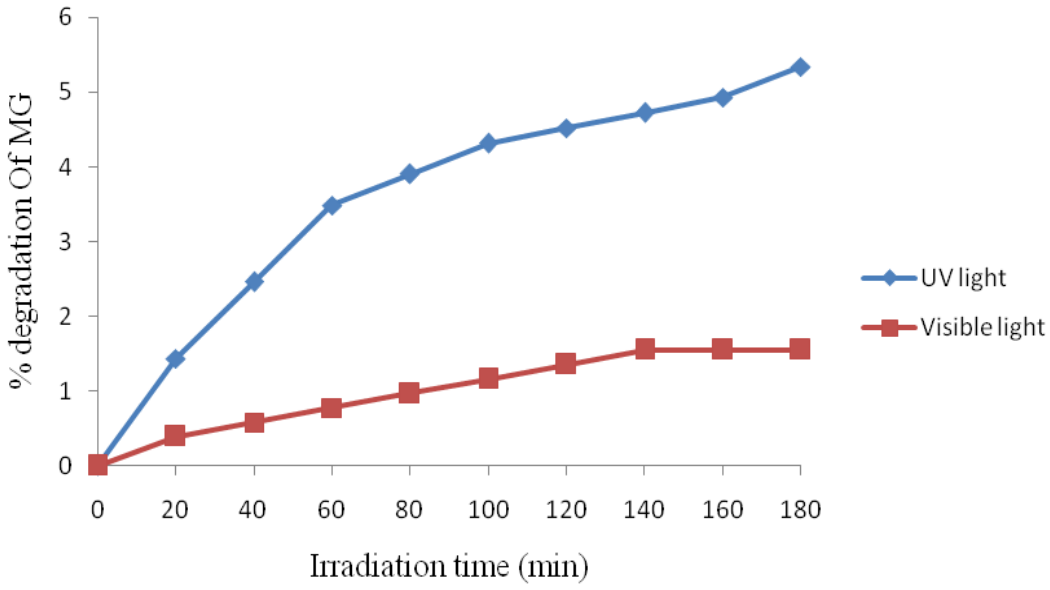

Figure 8. Plots of percentage degradation of MG dye as function of time under UV and Visible light irradiations in blank solution (without catalyst).

wavelength (nm) corresponding to absorption edge.

Accordingly, the band gap absorption edge of the $MnO_2/Al_2O_3/Fe_2O_3$ photocatalyst was the determined to be 630 nm, and thus corresponds to reduced band gap energy of 1.97 eV compared with E_g(eV) of Fe_2O_3 (2.3 eV). Such a reduction in the band gap energy may be the result of positive change in the crystallite phase and the size of ternary mixed oxide and defect of the composite structure. Therefore, the result indicates that the $MnO_2/Al_2O_3/Fe_2O_3$ nanopowder can have a suitable band gap for photocatalytic degradation of organic pollutant under visible light irradiation.

Photocatalytic degradation study

The photocatalytic activity of as-synthesized nanomaterial was evaluated by the degradation of malachite green dye in aqueous solution. The decolorization of the MG dye was examined under three different conditions (treatments): under UV and visible light irradiation without any catalyst (blank solution), in the presence of catalyst without light irradiation (in dark) and in the presence of $MnO_2/Al_2O_3/Fe_2O_3$ photocatalyst under UV and visible light irradiation, respectively. For the blank experiment (in the absence of the catalyst) under UV and visible light irradiation, almost insignificant degradation of the dye was observed (with only 3.4 and 4.2% decolorization efficiencies of the photocatalyst under visible and UV light irradiations, respectively). The percent adsorption values of MG dye is a function of time without the catalyst under visible and UV light irradiations. The corresponding plots of percent degradation as a function of time (under both visible and UV light irradiation) are shown in Figure 8.

In the presence of photocatalyst ($MnO_2/Al_2O_3/Fe_2O_3$), but without irradiation, only 6.98% decolorization efficiency was observed throughout the 180 min. This result confirms that degradation of the MG in the presence of the photocatalyst, but without light irradiation is insignificant. The fact is that no electron-hole pair could be generated in the semiconducting material without assistance of light irradiation (photoinduction). The formation of electrons and holes are responsible for enhancing the oxidation and reduction reactions with the malachite green dye, which might be adsorbed on the surface of the semiconductor to give the necessary products. Actually, the experimental results show that when the dye solution is exposed to UV and visible light irradiation for 180 min in the presence of $MnO_2/Al_2O_3/Fe_2O_3$ photocatalyst, about 69.30 and 92.89% of the MG dye could be degraded by UV and visible light irradiations, respectively. Accordingly, the degradation efficiency of MG dye under the visible light was found to be much larger than it was under the UV light irradiation. This enhancement under visible light in the presence of $MnO_2/Al_2O_3/Fe_2O_3$ photocatalyst could be explained from two reasons. The first one could be the fact that the $MnO_2/Al_2O_3/Fe_2O_3$ photocatalyst prepared by the sol gel method has a high specific surface area, that could give more active surface sites to adsorb water molecules and to form active •OH and HOO• radicals by trapping the photogenerated holes. This free active radical drive the photodegradation reactions and eventually leads to the decomposition of organic pollutants in aqueous solution (Bharathi et al., 2010).

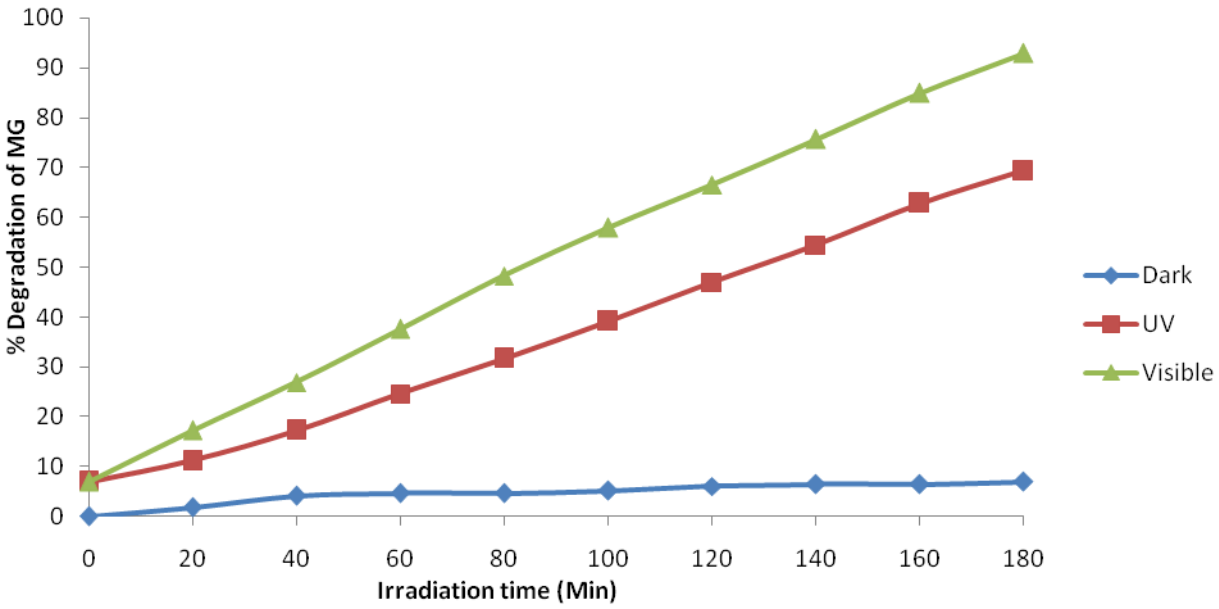

Figure 9. Plots of percentage degradation of malachite green dye as function of time (under UV, Visible and without irradiation) using $MnO_2/Al_2O_3/Fe_2O_3$ photocatalyst.

The higher surface area also facilitates the absorption of dye molecules on the surfaces of $MnO_2/Al_2O_3/Fe_2O_3$ photocatalyst. Under visible light irradiation, MG molecules are absorbed on the surfaces of nanocomposite and produced electrons. These electrons are captured by the surface adsorbed O_2 molecules to yield O_2•− and HO_2• radicals, which makes more chance to touch with dye molecules and giving a faster reaction speed then, the MG molecules could be mineralized in time by the super oxide radical ions. Therefore, it can be concluded that the smaller crystalline size of nanocomposite are favorable for the reduction of O_2 and oxidation of H_2O molecules by trapping electrons and holes, which improves the photocatalytic activity of the nanocomposites photocatalyst under visible light region.

The second reason could be the presumption that some of the Al (III) ions and Mn (IV) ions in the photocatalyst might be substituted by Fe (III) lattice site to form a stable solid solution. Such replacements of Al (III) and Mn (IV) ions by the Fe (III) ions can obviously create a charge imbalance (Ali Ismail, 2005). The charge imbalance must be satiated as Mn (IV) ions were reduced to Mn (III) ions. The existence of the Mn (IV) ions can thus inhibit the recombination of the photogenerated electron-hole pairs.

As a result, more OH^- ions would be adsorbed on the surface of the catalyst to overcome the charge balance. These OH^- ions present on the surface of the photocatalyst would accept the holes that are generated by the visible light illumination and thus converted to hydroxyl radicals (•OH), the radicals so formed can oxidize very easily the MG dye solution. On the other hand, the same visible light irradiation could be able to create oxygen vacancies on the structure of the photocatalyst structure. The oxygen vacancies formed as such can trap the electrons that are excited from the VB to the CB and thereby converted into superoxide radicals ($O•_2^-$) (Zhang et al., 2009). These $O^{\bullet}{}_2^-$ radicals are active enough to promote the oxidation of organic substances and effectively inhibited the electron-hole pair recombination. Therefore, these results show that the composite nanomaterial has a good photocatalytic performance in the degradation of MG dye in aqueous solution under visible light irradiation. The photodegradation values of MG dye as a function of time under UV and Visible light irradiations and without light irradiation are presented. Plot of percentage degradation as a function of time under UV, Visible and without irradiation are also shown in Figure 9.

Kinetic studies of photocatalytic degradation of MG

The adsorption of MG under without irradiation and its photocatalytic degradation under UV and Visible irradiations follow the pseudo first- order reaction kinetics expressed by the equation:

$$kt = \ln \frac{C_o}{C_t}$$

Where k is the reaction rate constant, C_0 is the initial concentration of MG solution and C_t is the concentration of MG solution at the reaction time t. The linear plot of $\ln C_o/C_t$ versus irradiation time *t* is shown in Figure 10 and values of rate constant (k) as a function of time is

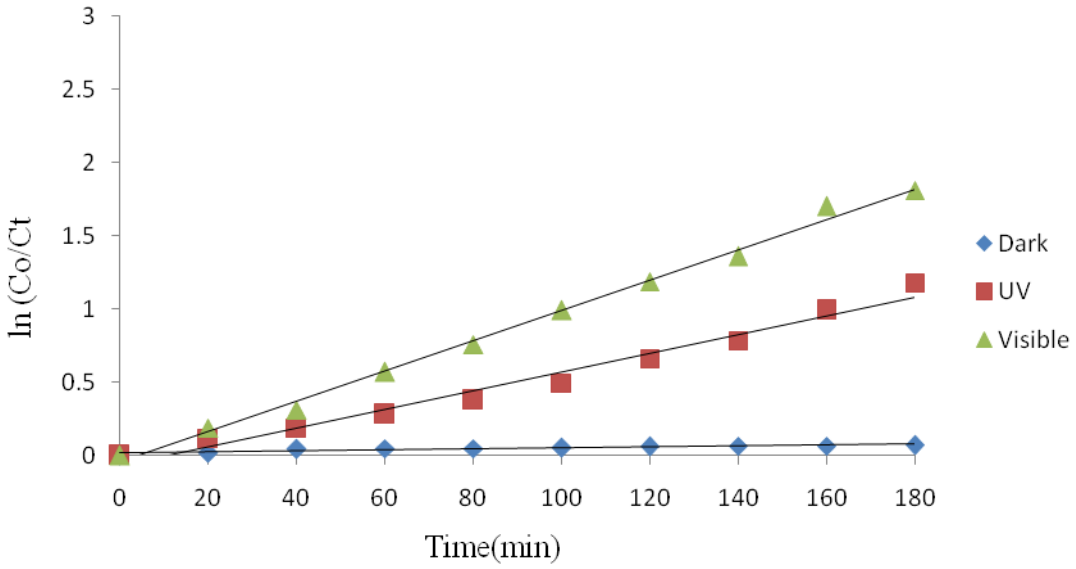

Figure 10. Plots of ln (C_0/C_t) vs. time for adsorption and photocatalytic degradation of MG in the presence of catalyst without irradiation, and under UV and Visible light irradiations.

Table 5. ln (C_0/C_t) as a function of time without irradiation, and under UV and Visible light irradiations in the presence of the photocatalysts.

Time(min)	ln(C_0/C_t) in Dark	ln(C_0/C_t) under UV	ln(C_0/C_t) under Visible
0	0.000	0.000	0.000
20	0.019	0.118	0.189
40	0.043	0.189	0.313
60	0.048	0.283	0.571
80	0.048	0.380	0.758
100	0.053	0.495	0.994
120	0.062	0.663	1.190
140	0.067	0.786	1.360
160	0.067	0.989	1.700
180	0.072	1.180	1.810

presented in Table 5. The calculated adsorption rate constant for MG using $MnO_2/Al_2O_3/Fe_2O_3$ photocatalyst without irradiation is 4×10^{-4} min^{-1}. The calculated rate constants for the degradation of this dye under the UV and visible light irradiations using the same catalyst were found to be 6.56×10^{-3} and 1.0×10^{-2} min^{-1}, respectively. Determination coefficients (R^2) of the pseudo-first order reaction without light irradiation, under UV and visible light irradiations were found to be 0.856, 0.976 and 0.995, respectively.

Comparison of binary and ternary photocatalytic activities

In order to explore the photocatalytic activity of the binary and ternary mixed oxides, various studies had been carried out to search ideal semiconductor photocatalyst for degradation of organic pollutants. The result is shown in Table 6. It can be seen that the photocatalytic activities of the ternary mixed oxide photocatalyst displays significantly high degradation ability for organic pollutants in aqueous solution. The improvement may be explained in terms of synergetic effect on the specific adsorption property and the efficient electron-hole separation at the coupled ternary mixed oxides photocatalyst interface. However, up till now no $MnO_2/Al_2O_3/Fe_2O_3$ coupled ternary photocatalyst has been reported for degradation of organic pollutants. These nanocomposite photocatalyst were found to be more photoeffective than binary Al_2O_3/Fe_2O_3 photocatalyst for oxidation of organic compound.

Table 6. Comparison of the photodegradation efficiency of organic dye in term of binary and ternary photocatalyst

Binary photocatalysts	Types of dye	Degradation efficiency (%)	Ternary photocatalysts	Types of dye	Degradation efficiency (%)
ZnO/Cu_2O	MO	73	$TiO_2{\cdot}[ZnFe_2O_4]_x$	Congo Red	90
Al_2O_3/Fe_2O_3	Bisphenal A	60	$Y_2O_3/Fe_2O_3/TiO_2$	EDTA	92
Fe_2O_3/TiO_2	MO	85	Fe_2BiSbO_7	MB	96.59
Al_2O_3/CeO_2	Congo red	80	Sr_2FeMoO_6	Acid Red B	100
$Al/Al_2O_3/TiO_2$	Cypermethrin	60.4	Ag/S/ZnO	MG	98
MnO_2/ZnO	MB	50	-	-	-

SUMMARY AND CONCLUSIONS

New composite nanosized $MnO_2/Al_2O_3/Fe_2O_3$ photocatalyst with a rhombohedral structure and oxygen vacancies was successfully synthesized by the sol-gel method by using metal salts as a starting materials. The as-synthesized materials were characterized by AAS, XRD, FTIR and UV/Visible spectroscopic techniques. The XRD pattern suggested that the as-synthesized nanopowders have a crystal structure with a good nonosized range of 20 to 26 nm particle sizes. Smallest particle size of catalyst was taken for characterization and photodegradation study of MG dye. Its band gap energy was about 1.97 eV, which is an important band gap for improving photocatalytic degradation of organic dyes in the visible region. The FTIR spectra before and after calcination are shown as -OH and Fe-O vibration bond in the as-synthesized photocatalyst calcinied at 400°C. Photocatalytic degradation of malachite green in aqueous solution was carried out under different conditions. It was included in the absence of the catalyst, under both UV and visible light irradiations (in blank), without light irradiation (in dark), and under both UV and visible light irradiations in the presence of the photocatalyst. The experimental results showed that higher decolorization efficiency was obtained under visible light irradiation in the presence of the catalyst. This may be due to the larger specific surface area, formation of oxygen vacancies and mixed valence states of manganese in the structure of the $MnO_2/Al_2O_3/Fe_2O_3$ photocatalyst.

Conflict of Interests

The authors have not declared any conflict of interests.

REFERENCES

Ali Ismail A (2005). Synthesis and characterization of $Y_2O_3/Fe_2O_3/TiO_2$ nanoparticles by sol–gel method. App. Cat. B: Environ. 58:115-121.

Baldrian P, Merhautova V, Gabriel J, Nerud F, Stopka P, Hruby M (2006). Decolorization of synthetic dyes by hydrogen peroxide with heterogeneous catalysis by mixed iron oxides. App. Cat. B: Env. 66:258-264.

Bharathi S, Nataraj D, Mangalaraj D, Masuda Y, Senthil K , Yong K (2010). Highly mesoporous α-Fe_2O_3 nanostructures: preparation, characterization and improved photocatalytic performance towards Rhodamine B (RhB). J. appl. Phy.43:015501 9p.

Brijesh P, Pardeep S, Jonnalagadda SB (2008). Visible light induce heterogeneous advancedoxidation process to degrade pararosanilin dye in aqueous suspension ZnO. Int. J. Chem. 47:830-835.

Chien-Tsung W (2007). Photocatalytic activity of nanoparticle gold/iron oxideaerogels for azo dye degradation. J. Non-Cry. Solids. 353:1126-1133.

Chu X, Zhang H (2009). Catalytic Decomposition of Formaldehyde on Nanometer manganese Dioxide. Mod. Appl. Sci. 3(4).

Cordier A, Peigney A, Grave ED, Flahaut E, Laurent C (2006). Synthesis of the metastable α-$Al_{1.8}Fe_{0.2}O_3$ solid solution from precursors prepared by combustion. J. Eur. Ceram. Soc. 26:3099-3111.

El-Moselhy MM (2009). Photo-degradation of acid red 44 using Al and Fe modified silicates. J. Hazard. Mater.169:498-508.

Gomathi DL, Murthya BN,Kumar SG (2009). Heterogeneous photo catalytic degradation of anionic and cationic dyes over TiO_2 and TiO_2 doped with Mo^{6+} ions under solar light:Correlation of dye structure and its adsorptive tendency on the degradation rate. Chem. 76:1163-1166.

Jia-feng W, Hai-tao W, Peng-yu Z, Ming-jing G (2011). Catalytic oxidation degradation of phenol in wastewater by heterogeneous Fenton reagent. J. Chong. University (English Edition) 10(4):1671-8224.

Kang M, Park ED, Kim JM, Yie JE (2007). Manganese oxide catalysts for NOx reduction with NH3 at low temperatures. Appl. Cats. A: Gen. 327:261-269.

Karakassides AM and Gournis D (2003). Magnetic Fe_2O_3–Al_2O_3 composites prepared by a modified wet impregnation method. J.Mater.chem. 13:871-876.

Kitis M, Kaplan SS 2007. Advanced oxidation of natural organic matter using hydrogen peroxide and iron-coated pumiceparticles. Chemical 68:1846-1853.

Laat JD, Le TG (2006). Effects of chloride ions on the iron (III)-catalyzed decomposition of hydrogen peroxide and on the efficiency of the Fenton-like oxidation process. Appl. Catal. B: Envion. 66:137-146.

Lei J, Liu C, Li F, Li X, Zhou S, Liu T, Gu M, Wu Q (2006). Photodegradation of orange I in the heterogeneous iron oxide–oxalate complex system under UVA irradiation. J. Hazard. Mater. B. 137:1016-1024.

Leland JK, Bard AJ (1987). Photochemistry of colloidal semiconducting iron oxide polymorphs. J. Phys. Chem. 91:5076-5083.

Li C, Zhang HJ, Chen ZQ (2010). Chemical quenching of positronium in Fe_2O_3/Al_2O_3 catalysts. Appl. Surf. Sci. 256:6801-6804.

Li FB, Li XZ, Liu CS,Liu TX (2007). Effect of alumina on photocatalytic activity of iron oxides for bisphenol degradation. J. Hazard. Mater. 149:199-207.

Mitta N, Shah A, Punjabi PB,Sharma VK (2009). Photodegradation Of Rose Bengal Using MnO_2 (Manganese Dioxide). Rasayan J. Chem. 2(2):516-520.

Neiva LS, Andrade MC, Costa CFM, Gama L (2009). Synthesis Gas (Syngas) production over Ni/Al_2O_3 catalysts modified with Fe_2O_3.

Braz. J. Petr.Gas. 3(3):083-091.
Park J, Lee Y, Khanna PK, Juna K, Bae JW,Kim YH (2010). Alumina-supported iron oxide nanoparticles as Fischer–Tropsch catalysts: Effect of particle size of iron oxide. J. Mol. Catal. A Chem.323:84-90.
Pattanayak CB (2010). Synthesis and Characterization of Alumina/Iron Oxide Mixed Nanocomposite. N. Int. Technol. Rourkela Rourkela 769008.
Rhoton FE, Bigham JM,Lindbo DL (2002). Properties of iron oxides in streams draining the Loess Uplands of Mississippi. Appl. Geochem. 17:409-419.
Sakthivel S, Shankar MV, Palanichamy M, Arabindoo B, Bahnemann DW,Urugesan V (2005). Enhancement of photocatalytic activity by metal depoitions: Characterisatsion and photonic efficiency of Pt, Au and Pd depoited on TiO_2 catalyts. Water Res. 38:3001-3008.
Su P (2010). Studies on Catalytic Activity of Nanostructure Mn_2O_3 Prepared by Solvent-thermal Method on Degrading Crystal Violet. Mod. Appl. Sci. 4(5).
Torres-Martinez LM, Juarez-Ramirez I, Ramos-Garza JS, Azquez-Acosta FV, Lee SW (2010). Bi_2MTaO_7 (M = Al, Fe, Ga, In) Photocatalyst for Organic Compounds Degradation under UV and Visible Light. WSEAS Trans. Environ. Dev.4(6).
Wang YC, Liua S, Li FB, Liu CP, Liang JB (2009). Photodegradation of polycyclic aromatic hydrocarbon pyrene by iron oxide in solid phase. J. Hazard. Mater.162:716-723.
Yan H, Pan W, An-Ping D, Jing Y, Ying-Ping H, Yong Y (2010). Preparation of CdS Nanoparticles with Reverse Micelle Method and Photo-degradation of malachite Green Dye. J. Ino. Mat. 25(11).
Zelmanov G, Semiat R (2008). Iron(3) oxide-based nanoparticles as catalysts in advanced organic aqueous oxidation. Water Res. 42:492-498.
Zhang G, Yang J, Zhang S, Xiong Q, Huang B, Wang J ,Gong W (2009). Preparation of nanosized Bi_3NbO_7 and its visible-light photocatalytic property. J. Hazard. Mater.172:986-992.
Zhao S, Wu HY, Song L, Tegus O, Asuha S (2009). Preparation of *c*-Fe_2O_3 nanopowders by direct thermal decomposition of Fe-urea complex: reaction mechanism and magnetic properties. J. Mater. Sci.44:926-930.